A New Affine Invariant Image Transform Based on Ridgelets

Esa Rahtu Janne Heikkilä
Department of Electrical and Information Engineering
P.O. Box 4500, 90014 University of Oulu, Finland
{erahtu,jth}@ee.oulu.fi

Mikko Salo
Department of Mathematics and Statistics / RNI
P.O. Box 68, 00014 University of Helsinki, Finland
mikko.salo@helsinki.fi

Abstract

In this paper we present a new affine invariant image transform, based on ridgelets. The proposed transform is directly applicable to segmented image patches. The new method has some similarities with the previously proposed Multiscale Autoconvolution, but it will offer a more general framework and possibilities for variations. The obtained transform coefficients can be used in affine invariant pattern classification, and as shown in the experiments, already a small subset of them is enough for reliable recognition of complex patterns. The new method is assessed in several experiments and it is observed to perform well under many nonaffine distortions.

1 Introduction

Often in computer vision applications we need to recognize objects or scenes viewed from various directions. Although this is a natural process for humans it has proven to be a difficult problem in computer vision. An common solution for this task is a combination of image segmentation, feature extraction, and recognition. In the segmentation step we try to extract a set of patches in a way that is insensitive to possible pose changes. For doing this there exists a wide range of possible approaches, going from simple thresholding to more sophisticated methods like mean-shift segmentation [1], similarity-measure-segmentation [2], and affine covariant area detectors [3], [4]. However, the optimal choice of the method depends heavily on the specific application.

In the case of successful segmentation we still have to deal with the geometric distortion induced by the view angle change. These distortions are usually well modeled by an affine transformation, and hence it is enough to design feature extraction techniques which eliminate this effect. The related methods may be divided into two main categories. The approaches in the first category use normalization to eliminate the affine changes and only then apply some feature extraction to the normalized patches. An example of such technique could be detection of ellipses using the Harris affine detector [3], which normalizes the ellipses to circles and then applies for instance the SIFT [5] operator to them. The

drawback in these approaches is the fact that the result becomes sensitive to the success of the affine normalization, which is generally difficult for arbitrary shaped patches. The methods in the second category apply affine invariant feature extraction to the patches directly, and the features are obtained without any normalization also in the case of patches with arbitrary shape. This paper proposes a new method for such feature extraction.

The first affine invariant feature extraction method, the affine invariant moments, was proposed already 40 years ago [6], though later corrected in [7] and [8]. Since then several other methods have appeared, including cross-weighted moments [9], trace transform [10], affine invariant spectral signatures [11], Multiscale Autoconvolution (MSA) [12] and spatial multiscale affine invariants [13]. The new technique we propose here is based on ridgelets [14] [15]. Ridgelets have recently attained a lot of interest in both mathematics and image processing [16] [17], due to their nice properties in describing objects containing straight lines. The new invariant introduced shares some similarities with Multiscale Autoconvolution, but the idea of using ridgelet type basis functions offers more variations and discriminating power. According to our knowledge no affine invariants based on ridgelets have been previously presented.

2 Motivation

The idea behind ridgelet-based affine invariants comes from the Multiscale Autoconvolution transform, which we discuss next. If $f : \mathbf{R}^2 \to \mathbf{R}$ is an image function, the MSA transform of f is defined by

$$Mf(\alpha,\beta) = \frac{1}{\|f\|_{L^1}^3} \int_{\mathbf{R}^2} \hat{f}(-\xi)\hat{f}(\alpha\xi)\hat{f}(\beta\xi)\hat{f}(\gamma\xi)\,d\xi, \tag{1}$$

where $\hat{f}(\xi) = \int_{\mathbf{R}^2} e^{-2\pi i x\cdot\xi} f(x)\,dx$ and $\gamma = 1-\alpha-\beta$. Using the inner product $(f,g) = \int_{\mathbf{R}^2} f(x)\overline{g(x)}\,dx$ we may write this as

$$Mf(\alpha,\beta) = \frac{1}{\|f\|_{L^1}^3} \int_{\mathbf{R}^2} (f, e^{-2\pi i x\cdot\xi})(f, e^{2\pi i\alpha x\cdot\xi})(f, e^{2\pi i\beta x\cdot\xi})(f, e^{2\pi i\gamma x\cdot\xi})\,d\xi. \tag{2}$$

This form produces affine invariants: $M(f\circ\mathscr{A}^{-1}) = Mf$ for any affine transformation $\mathscr{A}$. This is due to two facts. If f is replaced by the translation $g(x) = f(x-x_0)$, then $(g, e^{2\pi i x\cdot\xi}) = e^{-2\pi i x_0\cdot\xi}(f, e^{2\pi i x\cdot\xi})$, and the choice $\alpha+\beta+\gamma = 1$ makes the exponentials cancel in (2). Also, if f is replaced by $g(x) = f(A^{-1}x)$ where A is a 2×2 nonsingular matrix, then $(g, e^{2\pi i\delta x\cdot\xi}) = (f, e^{2\pi i\delta x\cdot A^t\xi})|\det A|$ for any $\delta\in\mathbf{R}$. If one makes the change of variables $\xi \mapsto A^{-t}\xi$ in (2) then the matrices and determinants cancel and we see that the expression is also invariant under composition with nonsingular matrices.

3 The new transform

The new ridgelet-based affine invariant transform is best understood by looking at the form (2). This form is invariant under replacing f by $f\circ A^{-1}$ since the analyzing element $e^{2\pi i\delta x\cdot\xi}$ is a function of the inner product $x\cdot\xi$ only. Then one obtains $(f\circ A^{-1}, e^{2\pi i\delta x\cdot\xi}) = |\det A|(f, e^{2\pi i\delta Ax\cdot\xi})$. Since $Ax\cdot\xi = x\cdot A^t\xi$ the matrix A may be removed by changing

variables $\xi \mapsto A^{-t}\xi$ in the ξ-integral. One then only needs to divide by a suitable power of $\|f\|_{L^1}$ to make the determinants cancel.

From the above we see that we can replace the analyzing elements $e^{2\pi i \delta x\cdot\xi}$ by other functions of $x\cdot\xi$, and the resulting forms will be invariant with respect to composition by matrices. We propose to use analyzing elements $\psi(\alpha x\cdot\xi-\beta)$, where $\psi:\mathbf{R}\to\mathbf{C}$ is a function (wavelet) in $L^1\cap L^\infty$ and $\alpha,\beta\in\mathbf{R}$. Define

$$\psi_{\alpha\xi,\beta}(x)=\psi(\alpha x\cdot\xi-\beta),$$

where $\xi\in\mathbf{R}^2$. Then $\psi_{\alpha\xi,\beta}$ has the shape of ψ (though scaled and translated) when restricted to lines parallel to ξ, and is constant in directions perpendicular to ξ. The function $\psi_{\alpha\xi,\beta}$ looks like a ridge, and such functions are called ridgelets in literature [14] [15]. We illustrate one example ridge in Figure 1.

So far we have only considered invariance with respect to $f\mapsto f\circ A^{-1}$, where A is a matrix. Translation invariance is achieved by shifting the image to its centroid. We will use $\tilde f(x)=f(x+\mu(f))$, where $\mu(f)=\frac{1}{\int_{\mathbf{R}^2}\chi_f(x)\,dx}(\int_{\mathbf{R}^2}x_1\chi_f(x)\,dx,\int_{\mathbf{R}^2}x_2\chi_f(x)\,dx)^t$, where $\chi_f(x)$ is the characteristic function of the support of the image f. We consider the following image transform.

Definition 1 *Let $f\in L^\infty(\mathbf{R}^2)$ be a compactly supported image function. We define*

$$If(\alpha_1,\alpha_2,\beta_1,\beta_2)=\frac{1}{\|f\|_{L^1}^2}\int_{\mathbf{R}^2}(\tilde f,\psi_{\xi,0})(\tilde f,\psi_{\alpha_1\xi,\beta_1})(\tilde f,\psi_{\alpha_2\xi,\beta_2})\,d\xi,$$

where $\alpha_1,\alpha_2,\beta_1,\beta_2\in\mathbf{R}$. In the case $\beta_1=\beta_2=0$, we also write

$$If(\alpha_1,\alpha_2)=If(\alpha_1,\alpha_2,0,0).$$

The most important property of the new transform is its affine invariance.

Proposition 1 *The transform $f\mapsto If$ is affine invariant: one has $I(f\circ\mathscr{A}^{-1})(\alpha_1,\alpha_2,\beta_1,\beta_2)=If(\alpha_1,\alpha_2,\beta_1,\beta_2)$ for any parameters $\alpha_j,\beta_j\in\mathbf{R}$ and for any affine transformation $\mathscr{A}$.*

Proof. If $g(x)=f(x-x_0)$ is a translated version of f, then the centered images $\tilde g$ and $\tilde f$ are the same. Consequently $Ig=If$ for all choices of the parameters.

Invariance with respect to composition by matrices also follows from the discussion above. Let $g(x)=f(A^{-1}x)$ where A is a nonsingular 2×2 matrix. Then one has $\mu(g)=A\mu(f)$ and $\tilde g(x)=f(A^{-1}(x+A\mu(f)))=\tilde f(A^{-1}x)$, and

$$\begin{aligned}(\tilde g,\psi_{\alpha\xi,\beta})&=\int_{\mathbf{R}^2}\tilde f(A^{-1}x)\bar\psi(\alpha x\cdot\xi-\beta)\,dx=|\det A|\int_{\mathbf{R}^2}\tilde f(x)\bar\psi(\alpha Ax\cdot\xi-\beta)\,dx\\&=|\det A|\int_{\mathbf{R}^2}\tilde f(x)\bar\psi(\alpha x\cdot A^t\xi-\beta)\,dx=|\det A|(\tilde f,\psi_{\alpha A^t\xi,\beta}).\end{aligned}$$

Since $\|g\|_{L^1}=|\det A|\|f\|_{L^1}$, we obtain

$$Ig(\alpha_1,\alpha_2,\beta_1,\beta_2)=\frac{|\det A|}{\|f\|_{L^1}^2}\int_{\mathbf{R}^2}(\tilde f,\psi_{A^t\xi,0})(\tilde f,\psi_{\alpha_1A^t\xi,\beta_1})(\tilde f,\psi_{\alpha_2A^t\xi,\beta_2})\,d\xi.$$

We make the change of variables $\xi \mapsto A^{-t}\xi$ in the last integral. The Jacobian is $|\det A|^{-1}$, and we obtain $Ig = If$ for all α_j and β_j.

There is some redundancy in the choice of the parameters $\alpha_1, \alpha_2, \beta_1, \beta_2$. This is seen in the following symmetries of the transform, which follow immediately from the definition by changes of variables.

Proposition 2 *(a)* $If(\alpha_1, \alpha_2, \beta_1, \beta_2) = If(\alpha_2, \alpha_1, \beta_2, \beta_1)$.

(b) $If(\alpha_1, \alpha_2, 0, 0) = \alpha_1^{-2} If(1/\alpha_1, \alpha_2/\alpha_1, 0, 0)$.

(c) $If(\alpha_1, \alpha_2, 0, 0) = \alpha_2^{-2} If(\alpha_1/\alpha_2, 1/\alpha_2, 0, 0)$.

We will mostly use the transform in the case $\beta_1 = \beta_2 = 0$, and in this case the symmetries indicate that it is enough to compute the values of $If(\alpha_1, \alpha_2)$ when (α_1, α_2) is in the triangle

$$T = \text{convex hull}\{(-1,-1), (-1,1), (1,1)\}. \tag{3}$$

We conclude by noting that the definition may be generalized to obtain other affine invariant transforms, which are of the form

$$I'f(\alpha_1, \ldots, \alpha_k, \beta_1, \ldots, \beta_k) = \frac{1}{\|f\|_{L^1}^{s-1}} \int_{\mathbf{R}^2} H((\tilde{f}, \psi_{\alpha_1 \xi, \beta_1}), \ldots, (\tilde{f}, \psi_{\alpha_k \xi, \beta_k}))\, d\xi.$$

Here we assume that $H : \mathbf{C}^k \to \mathbf{R}$ is a continuous function which is homogeneous of order $s > 2$, i.e. H satisfies $H(\lambda z_1, \ldots, \lambda z_k) = \lambda^s H(z_1, \ldots, z_k)$ for any $\lambda \geq 0$ and $(z_1, \ldots, z_k) \in \mathbf{C}^k$. Under these assumptions, the proof that $I'(f \circ \mathscr{A}^{-1}) = I'f$ for any affine transformation f proceeds analogously as the proof of Proposition 1.

4 Implementation issues

From now on we choose ψ to be real valued. When implementing the transform in Definition 1 we would need to evaluate inner products

$$\int_{\mathbf{R}^2} \tilde{f}(x) \psi(\alpha x \cdot \xi - \beta) dx, \tag{4}$$

with ξ in $\mathbf{R}^2$. This may be done efficiently using the Radon transform, similarly as in the case of the standard ridgelet transform [17] [18]. The advantage of this approach is easy to understand if we consider an example where the direction of ξ remains fixed, but its absolute value changes. This gives us a set of ridges which have the same orientation, but they differ by scale. Computing the values for each inner product (4) now involves summing over the same lines in the image, only weighting them differently. Now in the Radon transform these sums would already be computed and the inner products can be obtained just by weighting the sums according to scaled ridge. To see this more precisely we first change to polar coordinates $\xi \mapsto r\omega_\theta$, where $r \in \mathbf{R}_+$, $\omega_\theta = (\cos\theta, \sin\theta)^t$, and $\theta \in [0, 2\pi]$. The Jacobian is r and the inner products (4) will look like

$$\int_{\mathbf{R}^2} \tilde{f}(x) \psi(\alpha r x \cdot \omega_\theta - \beta) dx. \tag{5}$$

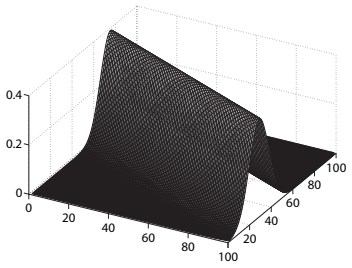

Figure 1: An example of a ridge function, using Gaussian wavelet.

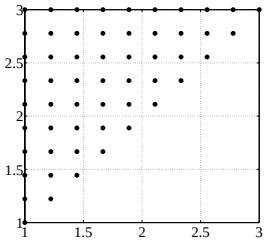

Figure 2: The (α_1, α_2) pairs used in the experiments.

If we further change variables in (5) so that $x \mapsto Tu$, where $u = (u_1, u_2)^t$ and T is the matrix

$$T = \begin{pmatrix} \cos\theta & -\sin\theta \\ \sin\theta & \cos\theta \end{pmatrix},$$

we will have (5) as

$$\int_{\mathbf{R}} \int_{\mathbf{R}} \tilde{f}(Tu)\psi(\alpha r u_1 - \beta)\, du_2\, du_1 = \int_{\mathbf{R}} \Big(\int_{\mathbf{R}} \tilde{f}(Tu)\, du_2 \Big) \psi(\alpha r u_1 - \beta)\, du_1. \tag{6}$$

The inner integral is the Radon transform of $\tilde{f}$,

$$\int_{\mathbf{R}} \tilde{f}(Tu)\, du_2 = \int_{\mathbf{R}} \tilde{f}(u_1\cos\theta - u_2\sin\theta, u_1\sin\theta + u_2\cos\theta)\, du_2 = R(\theta, u_1).$$

Substituting these to the invariant If we get

$$\begin{aligned} If(\alpha_1, \alpha_2, \beta_1, \beta_2) = \frac{1}{\|f\|_{L^1}^2} \int_0^{2\pi} \int_0^{\infty} \Big(\int_{\mathbf{R}} R(\theta, t_1)\psi(r t_1)\, dt_1 \Big) \\ \Big(\int_{\mathbf{R}} R(\theta, t_2)\psi(\alpha_1 r t_2 - \beta_1)\, dt_2 \Big) \Big(\int_{\mathbf{R}} R(\theta, t_3)\psi(\alpha_2 r t_3 - \beta_2)\, dt_3 \Big) r\, dr\, d\theta. \end{aligned} \tag{7}$$

From this we observe that the invariant can be computed by integrating the Radon transform at a fixed angle against scaled and translated ridges, by integrating over r, and finally by integrating over all the angles.

When discretizing the integrals in (7), we see that all integrals except the one over r are limited to a finite interval. However, as r increases the corresponding ridges become very narrow, which makes the coefficients at large values of r very small. So we will only consider coefficients in some circle centered at the origin, which we experimentally evaluated to be such that the smallest ridge widths were one image pixel. Also, since the coefficients with small r contribute more to the value of the invariant than coefficients with large r, we chose to use logarithmic sampling of r.

The symmetries in Proposition 2 indicate that if we set $\beta_1 = \beta_2 = 0$ we only need to take (α_1, α_2) from the triangle (3). Further, because we will choose ψ to be the symmetric Gaussian,

$$\psi(x) = \frac{1}{\sqrt{2\pi}} e^{-\frac{x^2}{2}}, \tag{8}$$

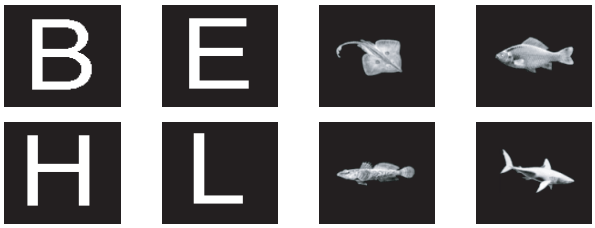

Figure 3: Some samples of the letter and fish images used in the experiments.

it is enough to consider the triangle $\{(0,0),(0,1),(1,1)\}$. However, we found that these values were not optimal for the implementation because for instance the inner products (6) converge slower if the α values are close to zero. We found it better to use larger α values and selected the 55 (α_1,α_2) pairs given in Figure 2. In addition, the fact that these values are in a uniform grid gives us a significant computational advantage, because the same inner products (6) will appear in several invariants and altogether we only need to evaluate them with scales $\alpha = \{1, 1.22, 1.44, 1.67, 1.89, 2.11, 2.33, 2.56, 2.78, 3\}$. The implementation for the ridgelet invariant we used is also available at the website: http://www.ee.oulu.fi/research/imag/msa/.

5 Experiments

In this section we assess the proposed transform (with $\beta_1 = \beta_2 = 0$, ψ is the Gaussian (8), and with the 55 (α_1,α_2) pairs in Figure 2) in several classification tasks. The achieved results are compared with affine invariant moments [19], Multiscale Autoconvolution [12] and cross-weighted moments [9]. These comparison methods were implemented as described in the given papers. For affine invariant moments we computed 4 and 60 independent invariants, for Multiscale Autoconvolution 37 invariants, and for cross-weighted moments 4 invariants using exponents $s = \{0.8, 0.95, 0.99, 1.05, 1.1, 1.2, 1.5, 1.07\}$. The reason for taking only 4 cross-weighted moments is their very high computational load, and thus taking more would have resulted in unreasonably long processing times. We will refer to these comparison methods as AMI4, AMI60, MSA, and CWM, respectively. The experiments were done using two different image sets, one having 100×100 binary images of 26 letters in the alphabet, and the other having 128×128 gray-scale images of 64 different fish. The gray-scale values in these images were scaled to the range $[0,1]$. We illustrate some samples of both image sets in Figure 3.

We first started with a simple test involving only the proposed method. We trained a nearest neighbor classifier using the images of 26 letters. Then we created a test set which contained 10 randomly affine distorted versions of each letter, a total of 260 images, and classified them. The resulting recognition rate was 99.2%, and the result verified the affine invariance in practice and showed that the implementation works.

However in real imaging situations we hardly ever encounter perfect affine transformations, and thus it is crucial that the methods are robust also against various nonaffine distortions. For this reason in the rest of the experiments we concentrate on examining the performance in situations where affine transformation is combined with various other distortions. To get a fairer comparison of the features we made the classifier to adapt to

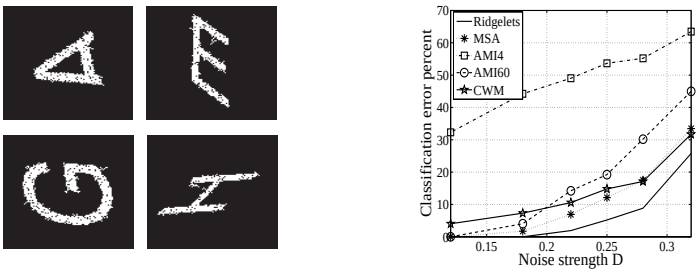

(a) (b)

Figure 4: Samples of distorted letter images with $D = 0.2$ (a) and corresponding classification results (b).

the feature space by extending the training set for all methods to contain the original images and 9 randomly affine transformed versions of each of them. The classification was then performed using a linear discriminant classifier, preceded by a principal component analysis if this was required for achieving a nonsingular covariance matrix.

5.1 Experiments with binary images using letter image database

When acquiring binary images, we typically face some binarization errors. To see how these distortions affect the different methods, we created a test set of letter images that contained 30 randomly affine transformed versions of each letter, disturbed with binary noise. We used additive uniformly distributed binary noise followed by filtering that removes small connected components. Some samples of the resulting test images are illustrated in Figure 4(a). The noise level D is the probability that a pixel is disturbed by noise before filtering. Figure 4(b) shows the results of this experiment, and it can be observed that the proposed method works fine even up to noise level $D = 0.25$, outperforming all the comparison techniques. Affine invariant moments seem to have the worst performance, though it is considerably improved when we use more of them.

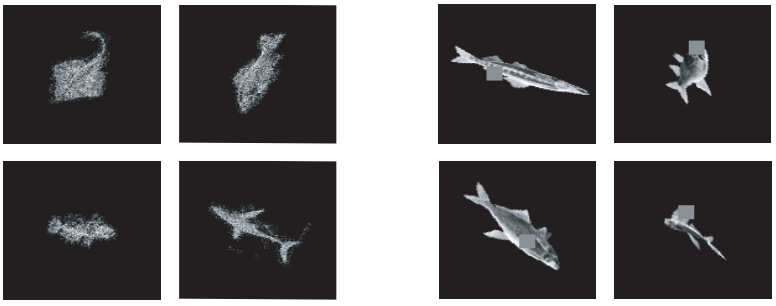

(a) Gaussian noise $\sigma = 0.2$. (b) Occlusion size 12.

Figure 5: Samples of noise distorted fish images.

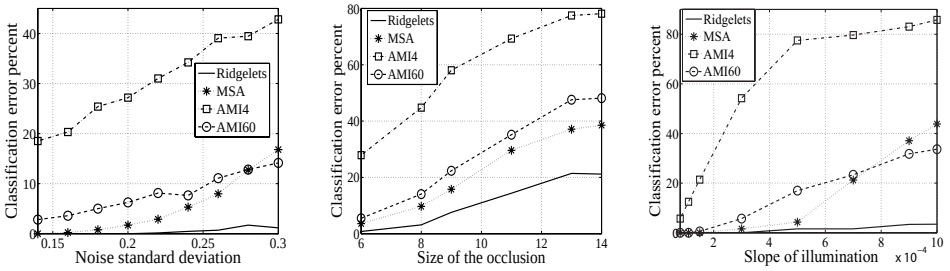

(a) Gaussian noise (b) Occlusion (c) Illumination

Figure 6: Classification results under Gaussian noise and occlusion.

5.2 Experiments with gray-scale images using fish image database

In most applications, recognition is done using gray-scale images. In this case there are several different sources for imaging errors, and to measure robustness against these we assess the methods in three different test settings, measuring the performance under Gaussian noise, occlusion, and nonuniform illumination. In each test we recognized 20 versions of each fish which had been disturbed by a random affine transformation and then by the given distortion. Unfortunately we had to omit the cross-weighted moments from this experiment, because the fish database had so many images with a large number of nonzero pixels that the computation times were prohibitively long.

In the first setting we tested robustness to Gaussian noise distortions, which usually model many error sources in e.g. CCD sensors. For testing we added random Gaussian noise having zero mean and different variations σ to images before classification. We illustrate some samples in Figure 5(a). The resulting classification errors with different methods are plotted in Figure 6(a). By looking at the results obtained here, one can see that the ridgelet approach is more accurate than the comparison methods, particularly at high noise values.

Another important error source are occlusions in the image. We tested this by introducing different sized and randomly situated occlusions on the fish images. The occlusion was a square shape, with uniform gray-value 0.5 and the center of the occlusion always on the fish. We show some samples of the resulting test images in Figure 5(b). The obtained results are shown in Figure 6(b). Despite the fact that large occlusions strongly disrupt the image intensity function, the proposed method makes only a few errors even up to occlusion size 8, and from there on outperforms the others with a clear difference.

In many situations it is very difficult, if not impossible, to arrange uniform lighting conditions. To see what kind of effects nonuniform lighting has to the recognition we created a lighting distortion so that starting from the vertical center line, to the left we linearly decreased the gray-scale values and to the right we similarly increased them. Figure 6(c) illustrates the results with several different slopes. Both MSA and ridgelet methods seem to give robust results up to the slope $5 \cdot 10^{-4}$, but from there on MSA collapses and only ridgelets offer reliable results.

6 Conclusions and future work

This paper introduces a novel affine invariant transform. The presented approach is based on ridgelets and it further gives rise to a framework for constructing a number of other affine invariant transforms. The invariants are efficiently implemented using the Radon transform and by proper selection of the transform coefficients. We assessed the method in experiments demonstrating several distortions appearing in photographing and binarization processes, and the new method gave strong performance. In general the results illustrate that ridgelet invariants extract highly discriminative and robust information from image patches. Interesting future research issues include finding optimal functions ψ and transformation parameters $\alpha_1, \alpha_2, \beta_1, \beta_2$. Based on the experiments and flexibility of the method, we believe that the novel framework introduced will offer a new practical and effective tool for affine invariant object recognition.

7 Acknowledgments

The authors would like to thank the Academy of Finland (project no. 110751), and Prof. Petrou and Dr. Kadyrov for providing us the fish image database.

References

[1] D. Comaniciu and P. Meer, "Mean shift: a robust approach toward feature space analysis," *IEEE Trans. Pattern Analysis and Machine Intelligence*, vol. 24, no. 5, pp. 603–619, March 2002.

[2] M. Fussenegger, A. Opelt, A. Pinz and P. Auer, "Object recognition using segmentation for feature detection," in *Proc. International Conference on Pattern Recognition*, vol. 2, Cambridge, England, 2004, pp. 41–44.

[3] K. Mikolajczyk and C. Schmid, "Scale and Affine invariant interest point detectors," in *IJCV*. 2004, 1(60) pp. 63–86.

[4] J. Matas, O. Chum, M. Urban, and T. Pajdla, "Robust wide baseline stereo from maximally stable extremal regions," in *Proceedings of the 13th British Machine Vision Conference*, Cardif, UK, 2002.

[5] D. Lowe, "Distinctive image features from scale invariant keypoints," in *IJCV*, 2004, 2(60) pp. 91–110.

[6] M.K. Hu, "Visual pattern recognition by moment invariants," *IEEE Trans. Information Theory*, vol. 8, pp. 179–187, February 1962.

[7] J. Flusser and T. Suk, "Pattern recognition by affine moment invariants," *Pattern Recognition*, vol. 26, no. 1, pp. 167–174, January 1993.

[8] T. H. Reiss, "The revised fundamental theorem of moment invariants," *IEEE Trans. Pattern Analysis and Machine Intelligence*, vol. 13, no. 8, pp. 830–834, August 1991.

[9] Z. Yang and F. Cohen, "Cross-weighted moments and affine invariants for image registration and matching," *IEEE Trans. Pattern Analysis and Machine Intelligence*, vol. 21, no. 8, pp. 804–814, August 1999.

[10] M. Petrou and A. Kadyrov, "Affine invariant features from the trace transform," *IEEE Trans. Pattern Analysis and Machine Intelligence*, vol. 26, no. 1, pp. 30–44, January 2004.

[11] J. Ben-Arie and Z. Wang, "Pictorial recognition of objects employing affine invariance in the frequency domain," *IEEE Trans. Pattern Analysis and Machine Intelligence*, vol. 20, no. 6, pp. 604–618, June 1998.

[12] E. Rahtu, M. Salo, and J. Heikkilä, "Affine invariant pattern recognition using multiscale autoconvolution," *IEEE Transactions on Pattern Analysis and Machine Intelligence*, vol. 27, no. 6, pp. 908–918, June 2005.

[13] E. Rahtu, M. Salo, and J. Heikkilä, "A new efficient method for producing global affine invariants," in *Proc. International Conference on Image Analysis and Processing*, Cagliari, Italy, 2005, pp. 407–414.

[14] E. J. Candés, *Ridgelets: Theory and applications, Ph.D. dissertation*. Stanford CA: Dept. Statistics, Stanford Univ., 1998.

[15] E. J. Candés and D. L. Donoho, "Ridgelets: A key to higher-dimensional intermittency?" *Phil. Trans. R. Soc. Lond. A.*, pp. 2495–2509, 1999.

[16] G. Chen, T. Bui, and A. Krzyżak, "Rotation invariant pattern recognition using ridgelets, wavelet cycle-spinning and Fourier features," *Pattern Recognition*, vol. 38, pp. 2314–2322, December 2005.

[17] M. N. Do and M. Vetterli, "The finite ridgelet transform for image representation," *IEEE Transactions on Image Processing*, vol. 12, no. 1, pp. 16–28, January 2003.

[18] X. J. Jun, N. Lin, and Y. Miao, "A new digital implementation of ridgelet transform for images of dyadic length," in *Proc. International Conference on Information Technology and Applications*, vol. 1, 2005, pp. 613 – 616.

[19] T. Suk and J. Flusser, "Graph method for generating affine moment invariants," in *Proc. International Conference on Pattern Recognition*, vol. 2, Cambridge, England, 2004, pp. 192–195.